Indian Journal of Pure & Applied Physics
Vol. 64, April 2026, pp. 369-376
DOI: 10.56042/ijpap.v64i4.20496

Structural, Dielectric, and AC Conductivity Studies of Silver-Doped Zinc Oxide/Polyvinyl Alcohol Nanocomposites

Praveen Kumar, Harsh Sharma, Virendra Singh & Praveen Malik*

Department of Physics, Liquid Crystal Lab, Dr B.R. Ambedkar National Institute of Technology, Jalandhar 144 008, India

Received: 9th June 2025; accepted: 9th February 2026

In this study, silver-doped zinc oxide nanoparticles (Ag-ZnO NPs) were synthesized via the hydrothermal method. The structural and chemical properties of the Ag-ZnO NPs were investigated using X-ray diffraction (XRD) and Fourier Transform Infrared Spectroscopy (FTIR). Surface morphology and optical characteristics were examined using field emission scanning electron microscopy (FESEM) and photoluminescence (PL) spectroscopy. The Ag-ZnO NPs exhibit a spherical morphology with an average particle size of ~ 66.0 nm. Polyvinyl alcohol (PVA)-based nanocomposite films incorporating Ag-ZnO NPs in varying concentrations (1.0, 5.0, and 10.0 wt.%) were prepared using the solution-casting method. The influence of Ag-ZnO NPs concentration on the dielectric properties and AC conductivity of PVA was systematically investigated. The results indicate that inclusion of Ag-ZnO NPs improvesthe dielectric permittivity and loss up to a critical concentration (1.0 wt.%). Beyond this threshold limit a reduction in permittivity, dielectric loss, and AC conductivity was also observed. Polarizing optical microscopy further confirmed the optical transparency of the nanocomposites, and its transparency is also affected by Ag-ZnO NPs.

Keywords: Silver doped zinc oxide, Polyvinyl alcohol, Nanocomposite, Dielectric permittivity, Dielectric, AC conductivity

1 Introduction

Polymer nanocomposites (PNCs) constitute a class of high-performance multifunctional materials composed of a polymeric host matrix reinforced with organic or inorganic nanoparticles (NPs) as nanofillers. Owing to their synergistically enhanced optical, electrical, mechanical, and chemical properties relative to their constituent materials, PNCs have attracted significant attention for emerging applications in electronic and optoelectronic devices[1-2]. In PNC systems, uniform dispersion of NPs within the polymer matrix is crucial for achieving improved functional performance. Among various polymer matrices, polyvinyl alcohol (PVA) is one of the most widely used polymers for nanocomposite fabrication due to its excellent film-forming ability, high flexibility, water solubility, ease of processing, optical transparency, non-carcinogenic nature, and dopant-dependent electrical properties[3-7]. Numerous studies have reported significant enhancement in the physico-chemical properties of PVA upon incorporation of different nanofillers, including metal oxide nanoparticles, carbon-based nanomaterials, and metallic nanoparticles[8-10]. The overall properties of PNCs depend not only on the intrinsic characteristics of the polymer and nanofillers but also on the interfacial interactions between them. Furthermore, the type, size, morphology, and concentration of nanofillers play a decisive role in tailoring the performance of nanocomposites, even when the polymer matrix remains unchanged[6-8]. These attributes make PVA an excellent host polymer for the development of tunable and application-specific nanocomposite systems. Among various metal oxide nanomaterials, zinc oxide nanoparticles (ZnO NPs) are n-type semiconductorsand belongto the II–VI group of the periodic table.ZnO NPshas been extensively investigated due to their multifunctional nature, non-toxicity, and suitability for applications in solar cells, sensors, optoelectronic devices, and biomedical fields[11-12]. Despite its promising characteristics, pristine ZnO NPs often exhibit limited performance. To overcome these limitations, doping with noble metals such as silver (Ag) has been shown to significantly enhance the structural, optical, electrical, and functional properties of ZnO, thereby improving its applicability compared to undoped ZnO NPs[13-16]. The Ag–ZnO/PVA nanocomposite system is particularly attractive because it integrates metallic (Ag), semiconducting (ZnO), and polymeric (PVA) phases within a single matrix, thereby enhancing antibacterial, photocatalytic, mechanical, optical, and

*Corresponding author: E-mail:malikp@nitj.ac.in

dielectric properties[17]. In recent years, PVA-based nanocomposites have been extensively explored due to their tunable physical properties and broad application potential. In the present work, Ag-doped ZnO nanoparticles were synthesized via a hydrothermal method, and their incorporation into the PVA matrix was systematically investigated. The influence of nanoparticle concentration on the structural, morphological, AC conductivity, and dielectric properties of the resulting Ag–ZnO/PVA nanocomposites has been examined and discussed in detail.

2 Experimental Details

2.1 Materials

Zinc nitrate hexahydrate ($Zn(NO_3)_2 \cdot 6H_2O$, 98%, Avra), silver nitrate ($AgNO_3$, analytical grade, Merck), sodium hydroxide (NaOH) pellets, Molychem), and polyvinyl alcohol (PVA; molecular wt. 89,000-98,000, Sigma-Aldrich). Allsolutions were freshly prepared in deionized (DI) water.

2.2 Synthesis of Silver Doped Zinc Oxide Nanoparticles

Ag-ZnONPs were synthesised using the hydrothermal method in which $Zn(NO_3)_2 \cdot 6H_2O$, $AgNO_3$, NaOH were used as precursors. 2.58 grams of $Zn(NO_3)_2 \cdot 6H_2O$ were dissolved in DI water (100ml) along with 0.147 grams (9 mol%) of $AgNO_3$ under continuous stirring at room temperature[18-19].1M NaOH solutionwas added dropwise to maintain pH to 11[20]. The final solution was sealed in Teflon cylinder insidea stainless steel autoclave reactor and then heated for 6 hr at 60°C.The greyish colour precipitates were collected and washed with DI and ethanol 2-3 times and then dried overnight. The final product was calcinated at 400°C for 4 hr[18-19]. Figure 1 shows a schematic synthesis of Ag-ZnO NPs.

2.3 Preparation ofNanocomposite (PVA/Ag-ZnO NPs)

A nanocomposite film comprising Ag-ZnO NPs dispersed in PVA matrix was prepared using solution casting method. Initially, PVA was dissolved in DI water under continuous stirring with a high-speed magnetic stirrer for 10-15 minutes. Once fully dissolved, Ag-ZnO NPs were added in different concentrations, 1.0 wt %, 5.0 wt %, and 10 wt% to the PVA solution.A wide range of Ag-ZnO NPs wasused to understand the doping effect on PVA. The prepared solution was further stirred for 20 minutes at55°C, followed by ultrasonication to get a uniform dispersion of Ag-ZnO NPs. The homogeneous solution so prepared was poured into petri dishes and dried overnight in an oven. This process provides PNCs films with varying concentrations of Ag-ZnO NPs[9]. The schematic representation of PNC's film fabrication process, real image of pure PVA and PVA/Ag-ZnO NPs films are shown in Fig. 2(a-b) respectively.

3 Characterization Techniques

The structural analysis of prepared NPs was done by XRD using "PANalytical EMPYREAN XRD" machine, with Cu-Kα (λ = 1.5406 Å) radiation in the range 20°–70°and step size 0.0170° at room temperature. The size and morphology of Ag-ZnO NPs were examined by FESEM ("SIGMA 500VP, Zeiss)". Microscopic images of NPs films were taken with the help of a polarizing optical microscope (POM) (LV100POL, Nikon Eclipse, USA). FTIR (Agilent carry 630 FTIR) was employed for the identification of functional groups. The dielectric properties of nanocomposites were also studied with the help of an impedance analyzer (Wayne Kerr, 6500B) in the frequency range of 20Hz- 1MHz. The PL spectra of both Ag-ZnO NPs and nanocomposite filmswere recorded with the help of a fluorescence spectrophotometer (Cary Eclipse, Agilent).

4 Results and Discussion

4.1 XRD Analysis

XRD is a powerful technique that allows the determination of the crystallographic structure and crystallite size of materials. This method provides valuable insights into synthesized nanomaterials'

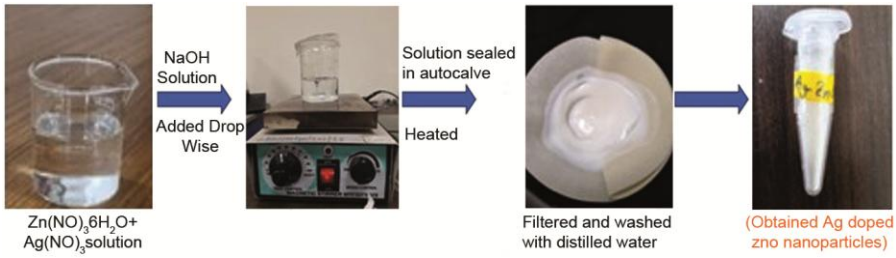

Fig. 1 — Synthesis of Ag-ZnO nanoparticles

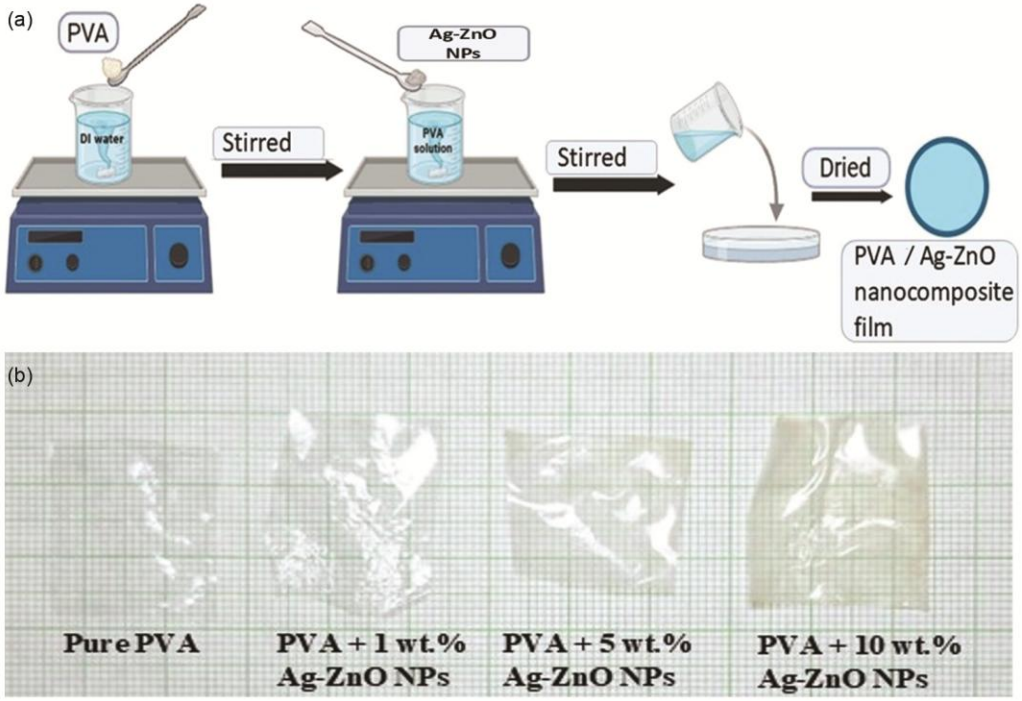

Fig. 2 — (a) Schematic representation of nanocomposite fabrication process; (b) Picture of fabricated nanocomposite films

purity and structural integrity by analysing the diffraction patterns. The XRD scan of the Ag-ZnONPs is presented in Fig. 3. The observed diffraction peaks at 2θ values of 31.81° (100), 34.48° (002), 36.25° (101), 47.52° (102), 56.58° (110), 62.92° (103), 66.39° (200), 67.94° (112), and 69.06° (201) correspond to the hexagonal wurtzite structure of ZnO. Additionally, the peak at 2θ = 39.09° (111) confirms the presence of silver. The high intensity and sharpness of the diffraction peaks indicate that Ag-ZnO NPs exhibits high crystallinity and purity. The XRD analysis confirms that Ag doping doesn't alter the crystal structure of ZnO. It is expected that Ag replaced itself with some of Zn atoms.The lattice parameters are also calculated with help of lattice geometry equation and expressed[21-22].

$$\left[\frac{1}{d^2} = \frac{4}{3}\left\{\frac{h^2+hk+k^2}{a^2}\right\} + \frac{l^2}{c^2}\right] \quad \ldots (1)$$

The calculated crystallite size (D) of the NPs is found~ 66.0 nm. The lattice parameters were also found as a = 3.24 Å, b = 3.24 Å, and c = 5.18 Å.

4.2 Textural Study

POM was used to examine the dispersion and morphology of the prepared nanocomposites. Figure 4 represents the microscopic images of nanocomposite films captured using POM ata

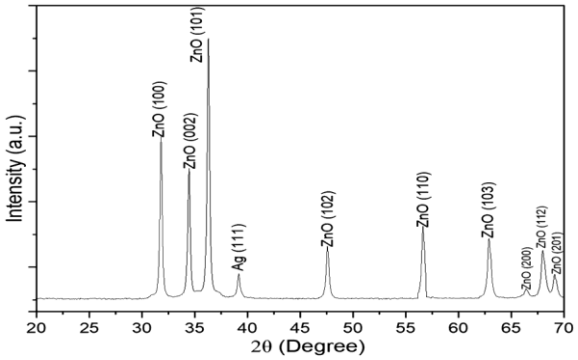

Fig. 3 — XRD pattern of Ag-ZnO nanoparticles

magnification of 10X and a scale bar of 100 µm. The prepared films weresandwiched between two ITO-coated glass substrates. Figure 4 (a) infers that the pure PVA film is highly transparent with no visible obstruction, indicating its uniformity and smooth texture. However, some dark sports were also seen. These spots may be due to the presence of Ag-ZnONPs which block the transmission of light through them and appear as dark spots inside the films. Figures 4 (b-d) show an increasing density of dark spots corresponding to Ag-ZnONPs embedded within the polymer matrix. As the concentration of Ag-ZnO NPs increases from 1to 5 wt % and 10 wt %, the number of dark spots increases significantly, indicates larger number of Ag-ZnO NPs.

4.3 FESEM Analysis

Morphological analysis of prepared Ag-ZnO NPs was done by FESEM and is shown in Fig. 5. Figure 5(a-b) shows that grown NPs are of spherical shape with high density. The diameter of the NPs was measured using ImageJ software and found to be ~ 66 nm. Figure 6 shows the histograms of count v/s diameter of Ag-ZnO nanoparticles.

4.4 Photoluminescence

Photoluminescence spectroscopy is used to investigate the electronic properties of semiconductor materials by analysing their light-emission behavior. In a typical PL process, incident photons with specific energy excite electrons to higher energy states; upon relaxation excited electron falls back to the ground state, by emitting photonsat characteristic wavelengths, giving rise to emission peaks in the PL spectra. Figures 7 and 8 represent PL spectra of pristine Ag-ZnO NPs and PVA/Ag-ZnO nanocomposite films, excited at wavelengths of 390 nm and 410 nm, respectively. The Ag-ZnO NPs exhibit a prominent emission peak at 446 nm, whereas pure PVA film shows an emission peak at 450 nm. In both spectra, the presence of secondary low-intensity peaks is attributed to the structural defects introduced by Ag doping in the ZnO lattice. Notably, in Fig. 8 the PL intensity of the nanocomposite films decreases with increasing the wt % of Ag-ZnO NPs. The observed decrease in photoluminescence intensity with increasing wt % of Ag-ZnO NPS in the PVA matrix is attributed to concentration quenching, and enhanced charge transfer to metallic Ag.At higher

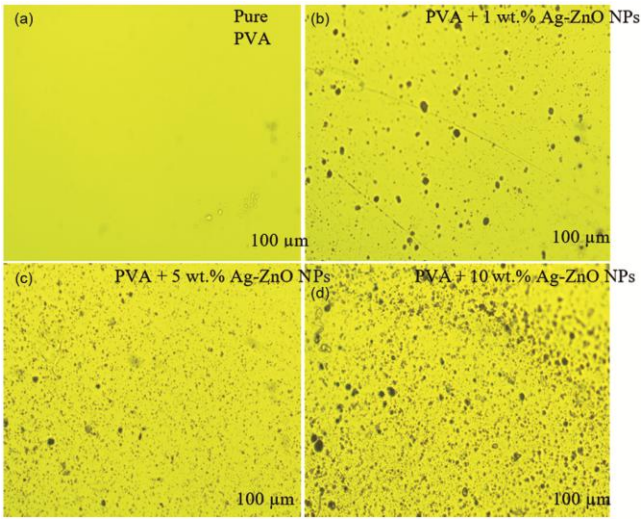

Fig. 4 — Microscope of (a) Pure PVA film, (b) PVA with 1.0 wt %Ag-ZnONPs, (c) PVA with 5.0 wt %Ag-ZnONPs; and (d) PVA with 10 wt %Ag-ZnONPs at room temperatureat 10X magnification in a parallel configuration of polarizer and analyzer

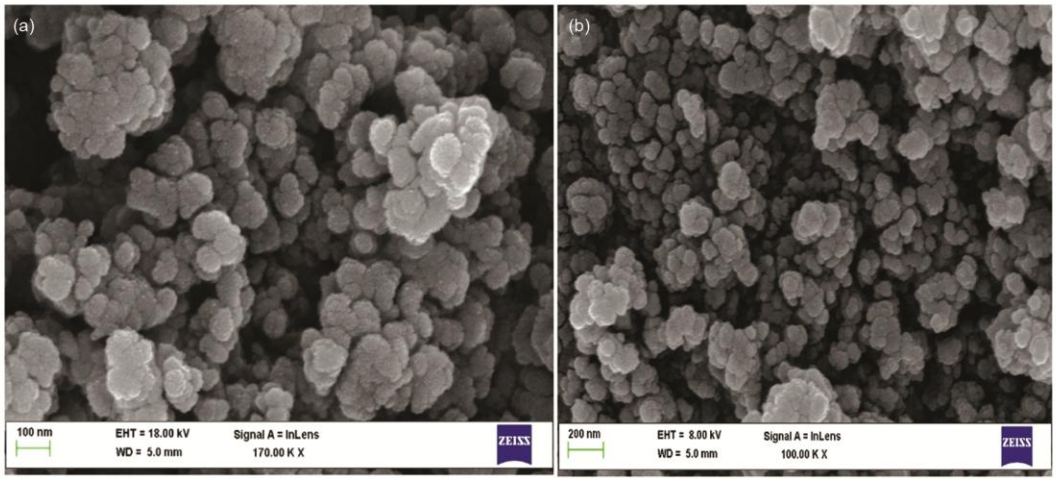

Fig. 5 — FE-SEM images of Ag-ZnO nanoparticles

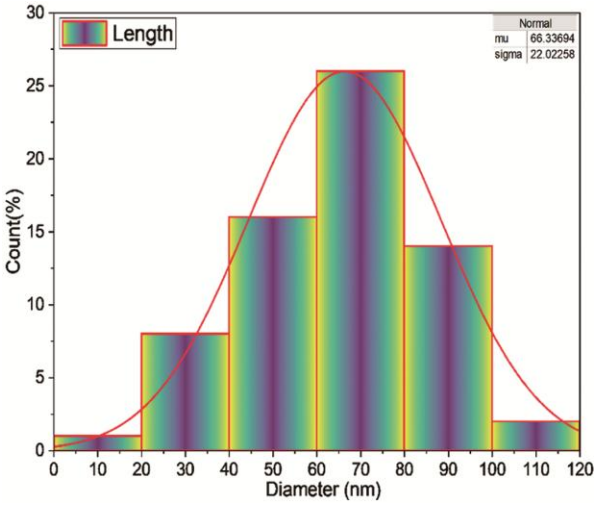

Fig. 6 — Particle size distribution of Ag-ZnO nanoparticles

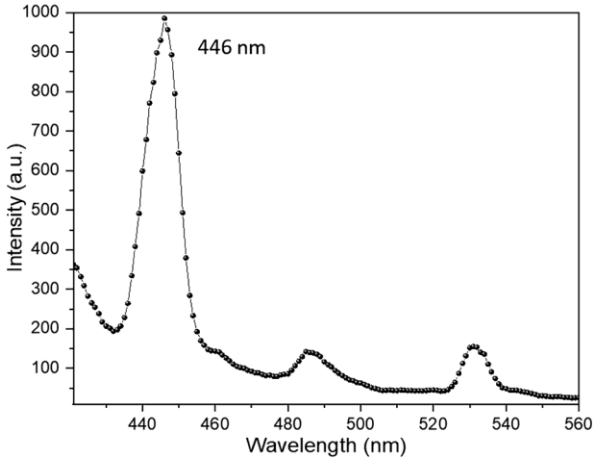

Fig. 7 — Photoluminescence spectra of Ag-ZnO nanoparticles

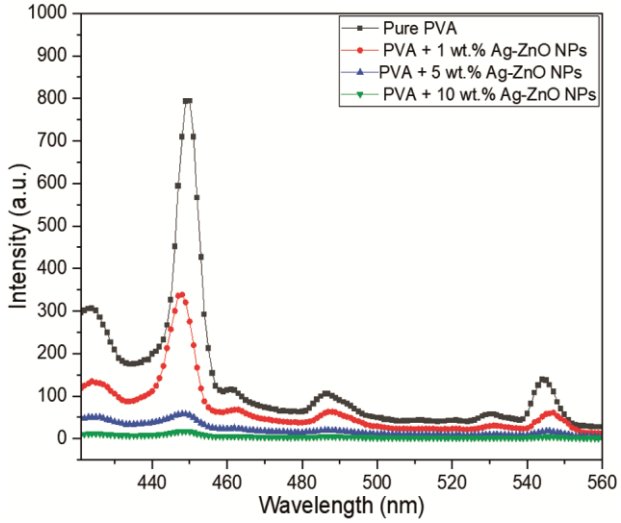

Fig. 8 — Photoluminescence spectra of pure PVA and PVA/Ag-ZnO nanocomposite films

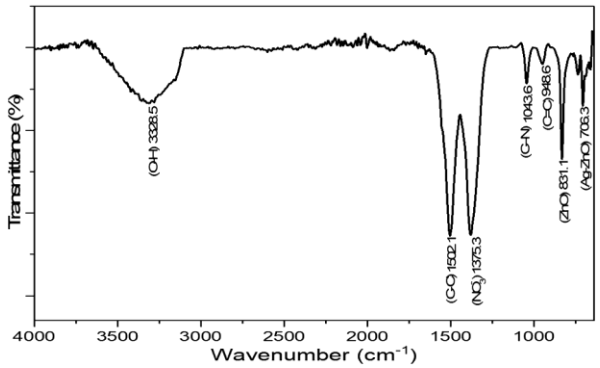

Fig. 9 — FTIR Spectrum of Ag-ZnONPs

concentrations of Ag-ZnO NPs additional defect states are created (e.g., oxygen vacancies, interstitials) at interfaces with the polymer. These defects act as non-radiative recombination centers that trap carriers and weaken the photoluminescence intensity. At higher concentration, closer proximity of NPs facilitates energy migration to quenching sites, reducing radiative recombination (concentration quenching). Additionally, charge transfer from ZnO to Ag NPs introduces electron traps that suppress PL emission[23-25].

4.5 FTIR

The presence of the functional group in the synthesized NPs was observed using FTIR analysis and shown in Fig. 9. The stretching band at 3328 cm^{-1} shows the presence of the O-H functional group, while the C-C stretching is shown by 1502 cm^{-1}. The bands at 1375 cm^{-1}, 1043 cm^{-1}, and 948 cm^{-1}belong to the vibrational modes of NO_3^-, C–N, and C=C groups, respectively. The stretching at 831 cm^{-1} is caused by ZnO, and Ag-ZnO bonding is indicated by a peak[16,21,26-28]at 706 cm^{-1}.

4.6 Dielectric Studies

The dielectric properties of PVA/Ag-ZnO NPs films were investigated using a capacitor like assembly consisting of two highly transparent ITO-coated glass substrates. The films were sandwiched between ITO substrates and electrical connections were made for dielectric measurement using indium ingots. The relative dielectric permittivity (ε′) was calculated using the equation[10],

$$\varepsilon' = (C \times d)/(A \times \varepsilon_0) \quad \ldots (2)$$

where C is the measured capacitance, d is the thickness of the film, A is the electrode area, and ε_0 is

the permittivity of free space. The dielectric loss (ε″) was also determined using the expression:

$$\varepsilon'' = \varepsilon' \times \tan\delta \qquad \ldots (3)$$

where $\tan\delta$ is the loss tangent.

Figures 10 and 11 represent the variation of frequency with ε′ and ε″, respectively, within a temperature range (30°C – 70°C) for pure PVA and PVA/Ag-ZnO NPs nanocomposites. It is seen from Figs. 10 (a-d) that that in low frequency region, ε′ is high and it decreases with increasing frequency. Higher value of ε′ at lower frequenciesoriginates from Maxwell–Wagner polarization, which typically occurs at the interfaces between insulator and conductor. At these interfaces, space charge or dipole accumulation gives rise to interfacial polarization[29-30]. At low frequency, space charges have sufficient time to respond and align with the applied electric field, whereas in the higher frequency region, changes in the electric field are too quick for the space charges to react, and the polarization effect is minimal or does not exist[31]. It is also found that doping of Ag-ZnO NPs increases the value of ε′ at 1.0 wt %. However, beyond the percolation threshold i.e. 1.0 wt % % in our case, ε′ decreases with increasing the concentration of Ag-ZnO NPs and can be seen in the Figs. 10(b-d). Once the percolation threshold is exceeded (> 1.0 wt %), a continuous network of doping NPs forms, dramatically decreasing the film's resistivity. Figure 11 showsa decrease in ε″ with increasing the frequency. It is noted that at lower frequencies, ε″ is too high. This high value is mainly due to the mobile charges linked with the polymer main chains. In contrast, at higher frequencies ε″ decreases as charges can't cope up with the variation of the electric field that results in a decrease of charge accumulation due to polarization[29]. Furthermore, it is also observed that both quantities ε′, ε″ increase with increasing temperature in each sample.This increase can be explained by polarization mechanisms influenced by thermal fluctuations. As temperature rises, intermolecular forces weaken, allowing dipoles

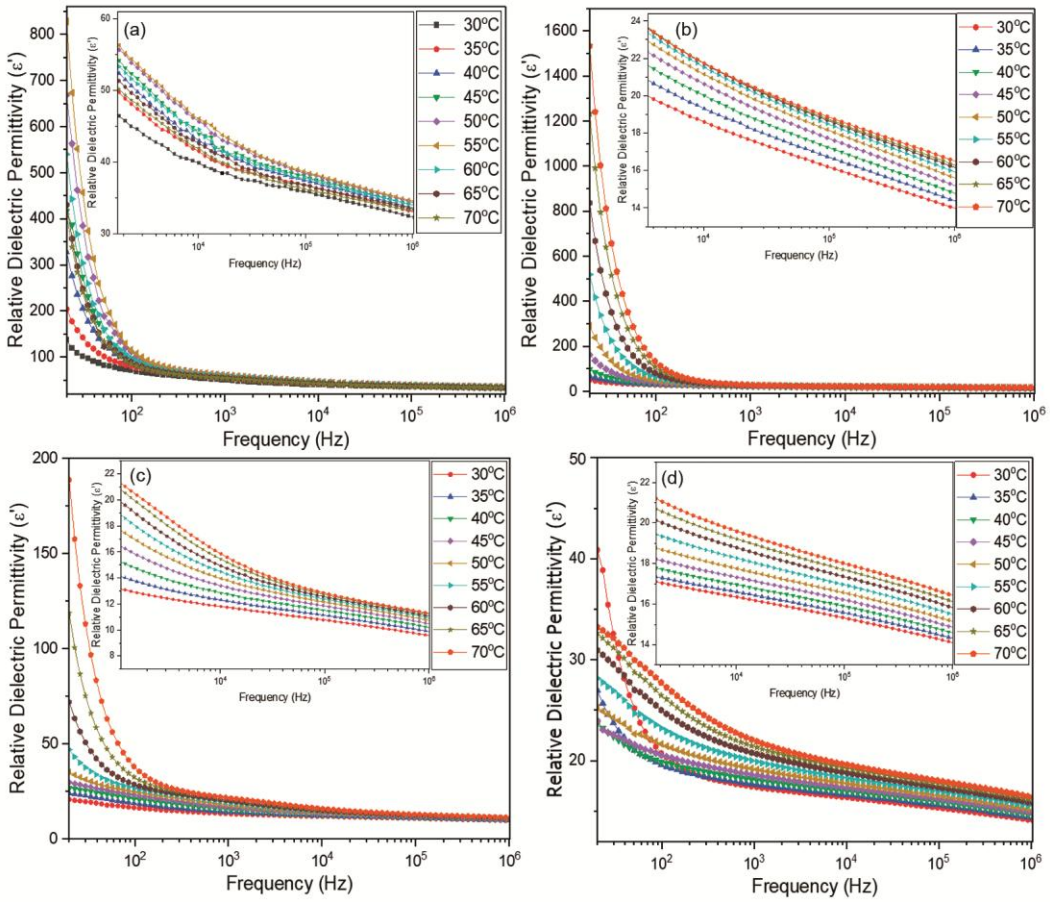

Fig. 10 — Relative dielectric permittivity of (a) Pure PVA film, (b) PVA with 1wt % of Ag-ZnO nanoparticles, (c) PVA with 5wt % of nanoparticles, (d) PVA with 10 wt % of Ag-ZnO nanoparticles

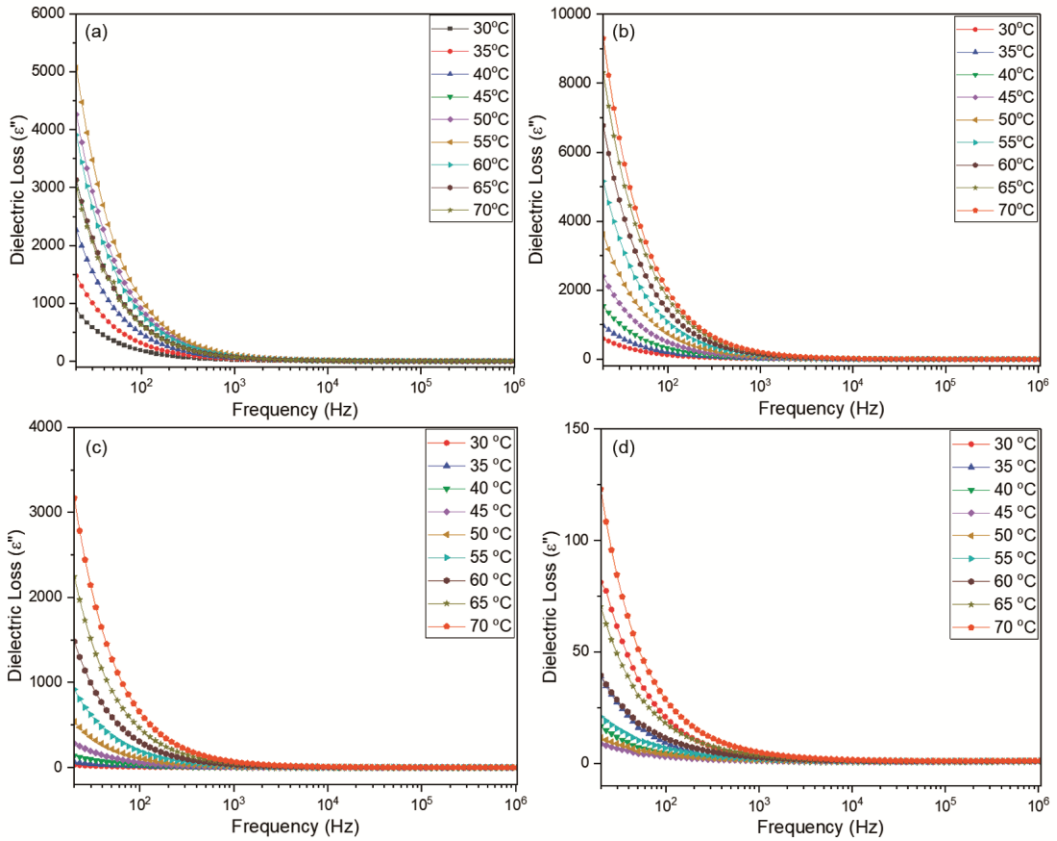

Fig. 11 — Dielectric loss of (a) Pure PVA film, (b) PVA with 1wt % of Ag-ZnO nanoparticles, (c) PVA with 5wt % of nanoparticles, (d) PVA with 10 wt % of Ag-ZnO nanoparticles

within the material to orient more readily inresponse to an external electric field, thereby enhancing permittivity. These findings are consistent with previous studies on PVA/ZnO and PVA/Ag nanocomposites[10, 29].

4.7 AC Conductivity

AC conductivity is the ability of a polymeric material to conduct alternating current when subjected to an external alternating electric field. The AC conductivity was calculated using the expression[11]:

$$\sigma_{ac} = 2\pi f \varepsilon_0 \varepsilon'' \qquad \ldots (4)$$

where f is frequency, ε_0 is the permittivity of free space (8.85×10^{-12} F/m^2). Figure 12 shows the effect of temperature on AC conductivity of pure PVA and PVA/Ag-ZnO nanocomposite films. The AC conductivity of the nanocomposite at 1.0 wt. % of Ag-ZnO NPs is higher than pure PVA film. This increasein conductivity is attributed tothe doping of Ag- ZnO NPs. Here Ag increases the number of free charge carriers in nanocomposites, which enhances the AC conductivity. However, at higher amount of

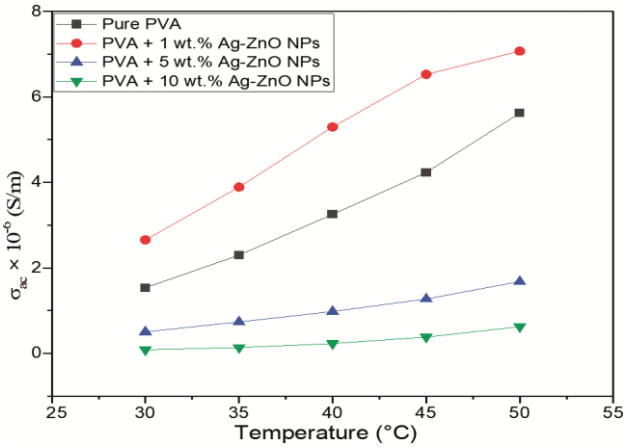

Fig. 12 — AC Conductivity of pure and nanocomposite films

Ag-ZnO NPs (above 1 wt. %), a decrease in AC conductivity is noticed. The observed decrease in conductivity at higher Ag–ZnO nanoparticle loadings (5 and 10 wt %) can be attributed to nanoparticle agglomeration within the polymer matrix. At elevated concentrations, Ag–ZnO NPs tend to cluster, leading to the formation of localized regions with high charge density. These higher charges will create a hindrance

in the path of moving charge, leading to a lower value of AC Conductivity[9-10].The value of AC conductivity for pure PVA and Ag ZnO NPs is also increased with an increase in temperature. It could be due to easy movement of charge carries through polymer at higher temperature[30]. The activation energy of pure PVA and PVA/Ag-ZnO films was calculated and found 0.51 eV, 0.41 eV, 0.56 eV, and 0.76 Ev, respectively using equation[12]:

$$\sigma_{ac} = \sigma_{\circ} exp\left(-\frac{E}{KT}\right) \quad \ldots (5)$$

$\sigma_{\circ}$ is a constant, K is Boltzmann constant, T is temperature and E is the activation energy. It is found that the nanocomposite with 1.0 wt % of AgZnO NPs is energetically higher, which is due to the easy movement of charge carriers[11, 31].

5 Conclusion

Here, Ag-ZnO NPswere obtained via a hydrothermal chemical route. Structural analysis confirmed the successful doping of Aginto the ZnO lattice without disrupting its intrinsic hexagonal Wurtzite structure. FE-SEM images revealed predominantly spherical nanoparticles with an average size of ~ 66 nm. Polarizing optical microscopy analysis indicated a decrease in the optical transparency of PVA-based nanocomposite films with increasing concentration of Ag-ZnO NPs. PL measurements indicate a reduction in emission intensity with increasing the wt % of Ag-ZnO NPs, suggesting suppressed electron–hole recombination and enhanced charge-carrier separation. The FTIR vibration band confirms the presence of various functional groups. Dielectric measurements revealed a strong correlation between the concentration of Ag-ZnO NPs and the electrical properties of the nanocomposites. An increase in the dielectric constant was observed with increasing the NPs content up to the percolation threshold (1.0 wt.%), beyond which a decline in ε′ is observed likely due to agglomeration effects. Additionally, dielectric permittivity increased with a rise in temperature and was attributed to the increased thermal activation of dipolar and interfacial polarization mechanisms. A significant enhancement in AC conductivity with temperature was also observed, with the maximum conductivity attained at an optimal value i.e. of 1.0 wt % of NPs. These findings demonstrate incorporating Ag-ZnO NPs into PVA matrices can effectively tailor dielectric performance, making these nanocomposites promising candidates for flexible dielectric layers and tunable permittivity applications in advanced electronic devices.

References

1 Dhatarwal P & Sengwa R J, *J Macromol Sci B Phys*, 59 (2020) 853.
2 Loste J, Lopez-Cuesta J M, Billon L, Garay H & Save M, *Prog Polym Sci*, 89 (2019) 133.
3 Shetty B G, Crasta V & Rajesh K, *AIP Conf Proc*, 2269 (2020) 030092.
4 Mahendia S, Tomar A K & Kumar S, *J Alloys Compd*, 508 (2010) 406.
5 Bhajantri R F, Ravindrachary V, Harisha A, Ranganathaiah C & Kumaraswamy G N, *Appl Phys A*, 87 (2007) 797.
6 Harun M, Saion E & Kassim A, *J Adv Sci Arts*, 1 (2009) 9.
7 Tuncer E, Sauers I, James D R, Ellis A R, Paranthaman M P, Goyal A & More K L, *Nanotech*, 18 (2007) 325704.
8 Ali MM, Abdelsalam SA, Hemeda OM, Sharshar T, Henaish AMA, *Optic Quant Elect*, 55 (2023) 95.
9 Menazea AA, Mostafa AM, Al-Ashkar EA, *J Mol Struct*, 1203 (2020)127374.
10 El-Shamy AG, *J Alloy Comp*, 810 (2019)151940.
11 Sharma K D, Skukla S, Sharma K K, Kumar V, *Mater Today Proc*, 49 (2022) 3028.
12 Wasly H S, El-Sadek M S A & Henini M, *Appl Phys A*, 124 (2018) 1.
13 Rafique S, Kasi A K, Kasi J K, Aminullah, Bokhari M & Shakoor Z, *Nanomater Nanotechnol*, 10 (2020) 1.
14 Umar A, Akhtar M S, Algadi H, Ibrahim A A, Alhamami M A M & Baskoutas S, *Molecules*, 26 (2021) 4619.
15 Amruth B A, Kushala C, Vaibhavi J G, Rashmi V & Sanjay K R, *Curr Nanomater*, 10 (2025) 93.
16 Kaur D, Bharti A, Sharma T & Madhu C, *Inter J Opt*, 2021 (2021) 1.
17 Chanu T S, Singh K J & Dev K N, *Poly Bull*, 81 (2024) 5069.
18 Kwon D & Kim J, *Korean J Chem Eng*, 37 (2020) 1226.
19 Kumar R, Rana D, Umar A, Sharma P, Chauhan S & Chauhan M S, *Talanta*, 137 (2015) 204.
20 Anbarasu M, Martin T M, Priya P, Vajiravelu S, Kumar M S K, Shaik M R, Kari Z A & Guru A, *Aquac Int*, 32 (2024) 5373.
21 Singh S, *Mater Today Commun*, 33 (2022) 104438.
22 CullityB D, *Elements X-Ray Diffraction*, (Addison-Wesley) (1956) p. 95.
23 Markevich I, Stara T, Khomenkova L , Kushnirenko V & Borkovska L, AIMS MatSci,3 (2016) 508.
24 Wagh S S, Kadam V S, Jagtap C V, Salunkhe D B, Patil R S, Pathan H M & Patole S P, *ACS Omega*, 8 (2023) 7779.
25 Xiong H-M, *J Mat Chem*, 20 (2010) 4251.
26 Nagasundari S M, Muthu K, Kaviyarasu K, Farraj D A A & Alkufeidy R M, *Surf Interfaces*, 23 (2021) 100931.
27 Panwar A & Yadav K L, *Mater Lett*, 309 (2021) 131469.
28 Naseer H & Iqbal T, *Biomass Convers Biorefinery*, 14 (2024) 21895.
29 Roy A S, Gupta S, Sindhu S, Parveen A & Ramamurthy P C, *Compos B Eng*, 47 (2013) 314.
30 Hemalatha K S, Sriprakash G, Ambika Prasad M V N, Damle R & Rukmani K, *J Appl Phys*, 118 (2015) 154103.
31 Ramesan M T, Jayakrishnan P, Sampreeth T & Pradyumnan P P, *J Therm Anal Calorim*, 129 (2017) 135.